JOURNAL OF MATERIALS SCIENCE 25 (1990) 3965–3975

Powder metallurgy aluminium alloys: characteristics of an Al–Cr–Fe rapidly solidified alloy

E. K. IOANNIDIS, T. SHEPPARD
Department of Materials, Imperial College of Science, Technology and Medicine, Exhibition Road, London SW7 2BP, UK

An Al–4Cr–1Fe alloy has been evolved utilizing the advantages of rapid solidification technology. The paper describes the formation of the as-atomized (inert gas) powder microstructure and its decomposition during *in situ* heating. It was observed that the most typical powder microstructure had a cellular morphology with a fine intercellular network consisting of iron-rich phases. Decomposition of the powder during *in situ* heating commenced from the intercellular network, finally resulting in a matrix with a high volume fraction of chromium-rich globular-like precipitates. Consolidation was achieved through cold compaction and hot extrusion; the alloy being easily extrudable. The room-temperature mechanical properties of the alloy were also assessed. The 0.2% proof stress and the tensile strength were below the target limits for dispersion-strengthened alloys, but the elongation and fracture toughness values were very promising. Finally, the extruded microstructure was related to mechanical properties.

1. Introduction

In recent years, significant interest has been directed to advanced aluminium alloys produced by the powder metallurgy (P/M)–rapid solidification (R/S) route. A specific target was the development of high-temperature dispersion-strengthened alloys capable of competing with titanium alloys on a strength basis over the temperature range 250 to 350° C [1]. These alloys could be utilized over a wide range of aerospace applications such as general structural applications (engine support, exhaust shield support, wheels), gas turbine engines (engine control, blades, vanes, compressor cases and low-temperature fan) and missile applications (rocket motor cases, fins, winglets, skins and support structures). Improvements in the processing conditions made the alloy's properties attractive in that tensile strengths of 450 to 600 MPa are achievable at room temperature, with an elongation to fracture and fracture toughness up to 17% and 25 MPa $m^{1/2}$, respectively, while at 315° C the tensile strength retained may be as high as 300 MPa. Among the most successful development alloy systems are those based on the aluminium–transition metal systems and especially Al–Fe–X [2, 3] and Al–Cr–X [4, 5] produced by several different atomization techniques. In these alloys, rapid solidification produces partitionless solidification, cellular/dendritic, microeutectic or icosahedral solidification structures that decompose during subsequent thermomechanical processing to produce alloys with the desired combinations of properties.

P/M Al–Fe–X alloys owe their strength to fine metastable Al_6Fe [6, 7] particles; however, structural heterogeneities and the initial high hardness create processing difficulties; moreover, the presence of the deleterious Al_3Fe phase, known to exist even in 10 μm powder particles [8], and the heterogeneity of the microstructure can result in loss of properties. On the other hand, the Al–Cr–Zr alloys are reported to be easier to fabricate [9] and attain strength from the precipitation of the coherent metastable phase $ZrAl_3$ ($L1_2$). Theoretical considerations suggested that combining the two systems and reducing the total solute should provide an easily consolidated material with high elevated temperature strength and improved fracture toughness. Hence an Al–4Cr–1Fe alloy produced by inert gas atomization and with inherently finer microstructure was expected to satisfy the required properties. The objectives of the present work were to study the solidification microstructure of this alloy and to examine the microstructural features of the extruded powder in relation to both strengthening and fracture behaviour.

2. Experimental procedure

The material was supplied by Metalloys, Sutton Coldfield, UK, in the form of inert gas atomized powder, produced by an up-draught technique. The chemical composition was Al–4.11 wt % Cr–1.04 wt % Fe–0.02 wt % Mn (analysed by the Imperial College Analytical Services Laboratory) having an experimentally calculated density of 2.770 Mg m^{-3} (compared to a theoretical density of 2.790 Mg m^{-3}). The particle size distribution, which was measured using a Malvern laser particle sizer, as well as an example of the morphology of the powder particles are illustrated in Fig. 1. The average powder

0022–2461/90 $03.00 + .12

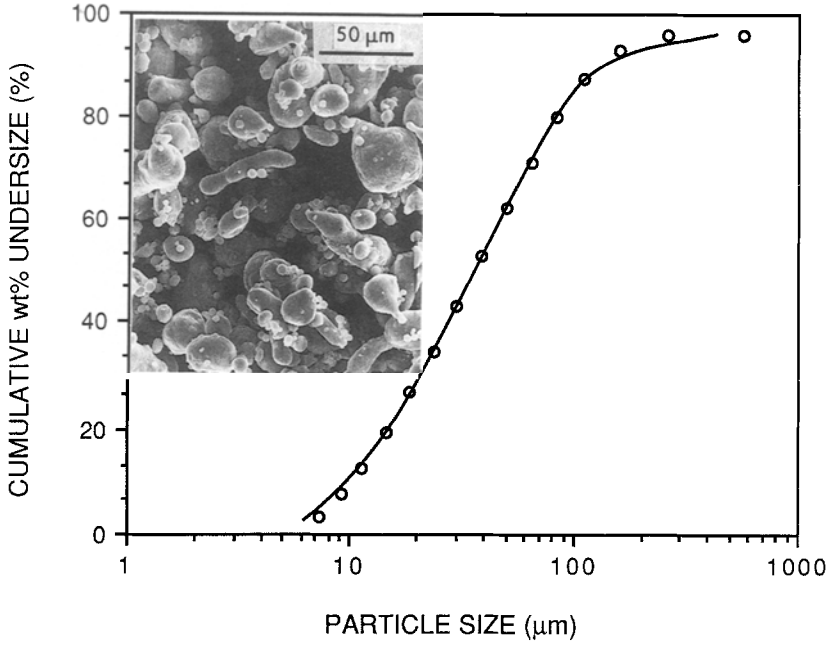

Figure 1 Typical powder morphology of alloy used (SEM) and size distribution.

particle size was measured as 35 μm; however, the data also depict the wide range in size typical of the as-atomized powders. Fig. 1 additionally shows a general characteristic of the atomized powders, i.e. the degree of sphericity increases with decreasing size, while the larger particles are almost ovoidal.

To enable a thorough study of the powder microstructure, nickel foils were impregnated with powder particles; the technique being described in detail elsewhere [10]. Subsequently, discs (3 mm diameter) punched from the foil, were mechanically ground to 50 μm thickness and electropolished in a solution of methanol with 5% $HClO_4$ and 31.67% 2-butoxyethanol at $-30°$ C and 20 V. The study was performed using a 1000 kV HVEM and a JEM-2000FX transmission electron microscope using a Links systems analyser incorporating a thin foil correction programme.

The fabrication of metal powders was performed in two distinct stages: cold compaction and hot extrusion. A double-action piston and tapered die assembly was used to cold compact 0.6 kg powder to approximately 94% density at a pressure of 500 MPa. Subsequently, the compacts were rapidly (3 to 5 min) preheated to the desired temperature and automatically transferred to the heated container of the hydraulic press, then extruded and water quenched. Extrusions were performed using a vertical action 5 MN ENEFCO press over a temperature range 400 to 550° C at 50° C intervals and an extrusion ratio of 20 : 1. For microstructural assessment, thin discs were prepared from the extrudates. They were then thinned using a conventional electropolishing jet technique in a methanol solution of 1.5% HNO_3 and 5% $HClO_4$ at $-40°$ C and 20 V.

To aid phase identification, X-ray analysis was conducted by using a Philips diffractometer with filtered Cu$K\alpha$ radiation on samples taken from the consolidated material as well as on samples from the as-atomized powder.

Tensile, hardness and short-rod fracture tests were performed on all as-extruded material produced. Standard Hounsfield no. 13 tensile specimens were machined and tested at a strain rate of 5.19×10^{-4} sec^{-1}.

3. Results and discussion

3.1. Powder microstructure and its decomposition during thermal exposure

The HVEM study of the powder revealed the overall features of atomized microstructures, which are illustrated in Fig. 2. Some powders exhibited either structurally featureless or cellular morphologies, but the most commonly seen microstructures exhibited a mixture of both morphologies. While rapid solidification techniques have the potential to extend considerably the solid solubility limits of various alloying elements in aluminium, the thermal gradients and interface velocities prevalent in these gas atomized powders are not sufficient to prevent complete solute segregation. Thus, solute segregation occurring upon solidification results in cellular solidification. Obviously the different morphologies can be classified in relation to the powder particle size. The smaller powder particles, 5 to 10 μm (see Fig. 2a), exhibited a higher proportion of segregation-free solid, while the coarser particles (Fig. 2b) were generally cellular with the cells elongated towards the direction of the solidification front. Larger particles frequently showed multiple nucleation sites, indicating that coarse powders are most likely to develop polycrystalline microstructures.

The solidification behaviour can be interpreted in terms of solidification mechanisms. Solidification occurs heterogeneously at the periphery of the liquid droplet, which is the reason why the powder particles, regardless of their size, are surrounded by a segregation-free rim, see Fig. 2b. At this stage, the solidification regime is governed by the degree of undercooling achieved prior to nucleation and thus a smooth solidification front produces the segregation-free rim. The size of this rim depends upon the degree of undercooling and the size of the liquid droplet. Subsequently, due to recalescence, the solidification front breaks up into a cellular one at a growth rate depending upon the heat extraction to the surroundings (cooling

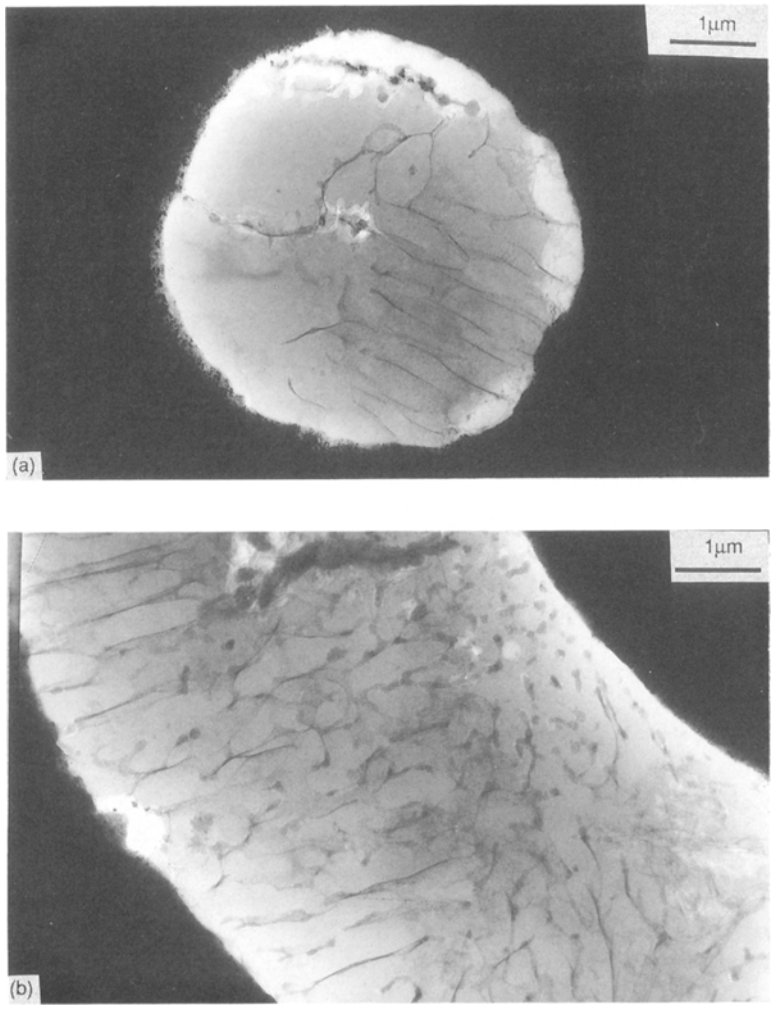

Figure 2 Microstructures of the as-atomized powder (HVEM).

gas). Instances of homogeneous nucleation have been detected, especially in larger droplets, in which chromium-rich phases have been formed within the liquid droplet. However, the abundance of heterogeneously nucleated droplets indicates that formation of nucleants has mainly been suppressed due to the degree of undercooling achieved. Clearly an increase in the liquid droplet size encourages the probability of solidification being affected by homogeneously nucleated second-phase particles.

X-ray examination, conducted on a typical powder sample, indicated that apart from α-Al, the equilibrium phase Cr_2Al_{13} (ASTM 29-14) was formed during rapid solidification. Moreover, a number of unassigned reflections, see Table I, were detected, a phenomenon which is common in rapidly solidified (R/S) aluminium alloys, probably attributable to iron-rich phases. To aid phase identification, and especially to determine the distribution of the alloying elements within the powder particles, STEM microanalysis has been carried out using a JEM-2000FX microscope, the results of which are illustrated in Table II.

Obviously, the matrix is depleted of iron, because iron diffuses to the intercellular network, forming the metastable $FeAl_6$ phase, which could be predicted from the eutectic systems [11]. The chemical composition of the phases at the intercellular network is different from the theoretical chemical composition of the $FeAl_6$ (74.35 wt % Al, 25.65 wt % Fe), which can be attributed to contributions from the adjacent matrix. Evidence supporting the latter proposition is well illustrated by analysing junctions of three cells (triple points), see arrowed example in Fig. 3, where the contributions from the adjacent matrix are significantly lower. X-ray diffraction techniques are unable to identify the phases present in the intercellular network because they are extremely fine and the volume fraction of the phases present is inadequate to give reflections of higher intensity than the background signal. Fig. 2b and Table II also indicate the presence of chromium-rich globular phases within the cells, being in agreement with the predicted behaviour of peritectic systems (i.e. the Al–Cr system), in which the formation of high-temperature peritectic phases prior to solidification can be expected. At some instances, coarser chromium-rich phases can be discerned at the interfaces, suggesting that these phases, formed prior to solidification, prevented cellular growth. Finally, it should be noted that different powder microstructures may show varying solute levels; particularly those exhibiting a segregation-free type of structure which is more common in smaller particles, where solute trapping is promoted.

Consolidation of the rapidly solidified powders involved thermomechanical working by extrusion, as

TABLE I *d*-spacings attributed to unidentified phases

d-spacings	258.5	243.4	229.8	229.5	228.4	227.1	223.9	223.5	126.4

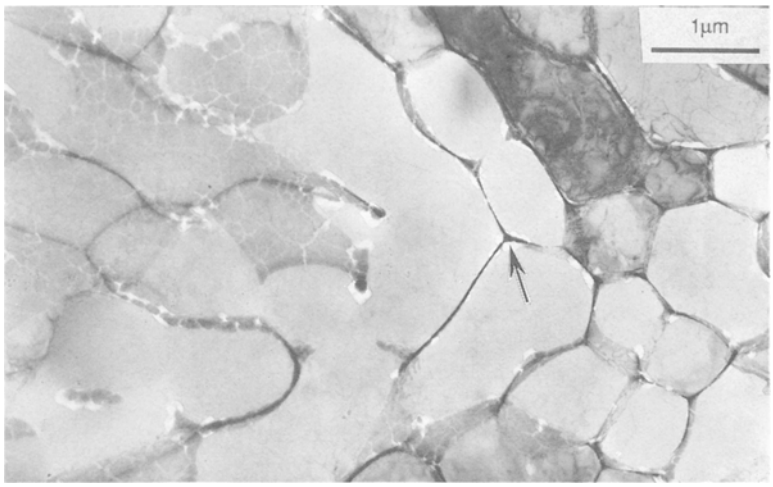

Figure 3 Cellular powder morphology (JEM 2000FX).

will be discussed later, which required prolonged exposure to high temperatures coincident with the application of high pressures, resulting in modification of the powder microstructure. To investigate the effect of heating alone, it was necessary to isolate the effects of heating from hot working. Hence, *in situ* heating of powder foils, conducted in the HVEM, revealed information concerning the effect of thermal treatment on the powder microstructure. The rapid heating (6 min) at 450° C did not have any major effect on the microstructure, Fig. 4a. After 8 min, small discrete precipitates which nucleated homogeneously within the chromium-rich matrix could be discerned, while a rapid growth rate of the precipitates in the intercellular network has been noted, see Fig. 4b. After 24 min the transformations have progressed further; the cells are now decorated with small globular-like precipitates, whilst plate-like precipitates (iron-rich) can also be observed in the intercellular network. After 46 min the precipitates are coarser and the plate-like precipitates spheroidize; moreover, at this stage, the cell boundaries can hardly be discerned (Fig. 4c).

The observations made during heat treatment indicated the following important features. Firstly, decomposition of the powder microstructure originates at the intercellular network by growth of the existing iron-rich precipitates which act as nuclei. Secondly, homogeneous nucleation within the iron-depleted cellular matrix leads to the formation of globular precipitates. Finally, during heating, all the precipitates coarsen at a relatively high rate, regardless of their chemical composition. Thus, it appears that despite the retention of chromium in solid solution during atomization (cellular solidification, see Table II), few benefits might be gained, as far as the mechanical properties of the consolidated product at elevated temperatures are concerned, unless the mode of precipitation can be either controlled or modified by adding other alloying elements, e.g. zirconium. Alternatively, the alloy could require processing at lower temperatures with the associated higher extrusion pressures. Obviously, it should be noted that the kinetics of phase transformations increase when the combined effects of pressure and temperature during the thermomechanical extrusion process are encountered.

3.2. Extrusion characteristics

Obviously, the most important step of alloy development research involves the assessment of the mechanical properties after consolidation. The extrusion process is usually the main consolidation route especially in forming high-strength powder alloys, because it is simple and combines both consolidation and hot working in one operation. The most important variables in extrusion are the initial billet temperature, ram speed and the reduction ratio. In the present work it was decided to maintain the ram speed constant at approximately 6.0 mm sec^{-1} and to use a reduction ratio of 20 : 1. Thus, the role of temperature on the extrusion characteristics and mechanical properties of the alloy was established.

It is usual, that with increasing extrusion temperature the maximum pressure required to initiate extrusion as well as the peak increment (the additional pressure required to establish a quasi static deformation zone) decrease, see Fig. 5, due to the decrease in flow stress resulting from the increase in temperature. It must be noted that the pressure required to initiate extrusion is a very important practical factor because it determines the highest pressure require-

TABLE II EDX microanalysis results

Location	Al (wt %)	Si (wt %)	Cr (wt %)	Fe (wt %)
Matrix	94.41 ± 0.95	0.95 ± 0.08	4.45 ± 0.25	0.20 ± 0.05*
Cellular interface	73.86 ± 0.46	1.97 ± 0.08	3.70 ± 0.10	20.46 ± 0.40
Triple point	67.05 ± 0.33	2.66 ± 0.21	3.73 ± 0.12	26.58 ± 0.25
Globular precipitates within cells	89.96 ± 1.31	1.11*	6.06 ± 0.11	3.43 ± 0.41
Coarse precipitates at interface	78.01	1.01*	14.02	6.96

*Data without statistical value, (for indication only).

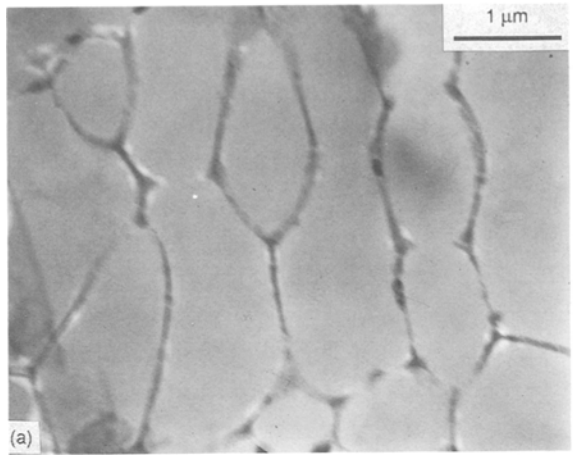

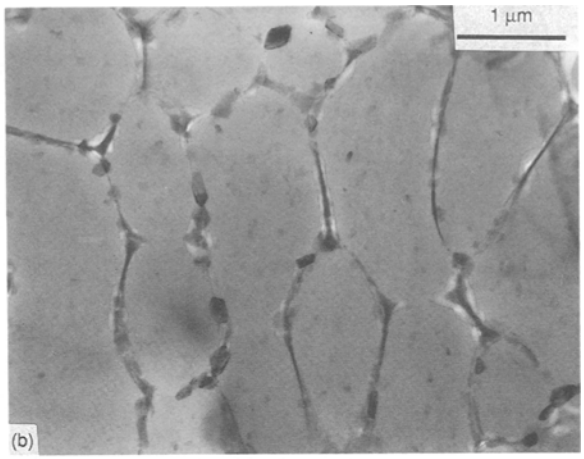

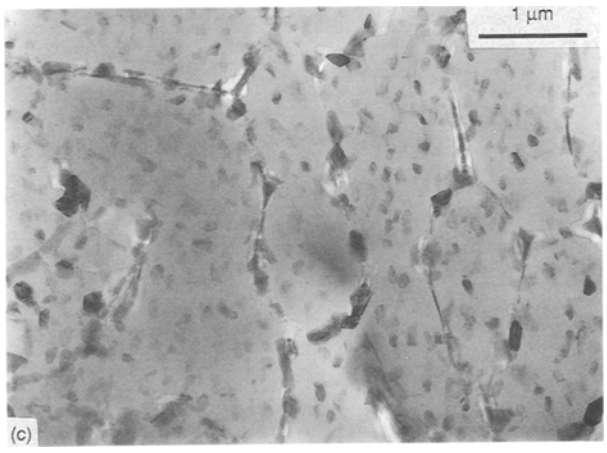

Figure 4 Structural changes during *in situ* heating of powder specimens: (a) 450° C, just after the heating up period (6 min); (b) 8 min at 450° C; (c) 46 min at 450° C.

ments and therefore the capacity of the press required. In the present investigation, the additional increment of extrusion pressure can be seen to be of moderate significance, because it has resulted in an increase of less than 23% over the steady state pressure. In other rapidly solidified powder metallurgy (RS/PM) high-temperature aluminium alloys, the peak increment constitutes 40% to 50% of the overall pressure [12, 13] indicating that this alloy has fewer obstacles to dislocation movements and thus could clearly be considered as a good matrix for further alloy development, e.g. reducing the content of chromium to reduce the fraction of coarse chromium-rich precipitates and/or introducing zirconium as a precipitation strengthening element. The moderate value of peak increment would be expected because *in situ* heating of powder samples revealed rapid precipitation and coarsening behaviour resulting in a microstructure composed of a high volume fraction of mainly coarse globular precipitates.

Finally, the extrusion pressure is related to the energy absorbed during plastic deformation and thus to the temperature rise during extrusion. Table III illustrates the initial billet temperature, the temperature of the billet when the peak pressure is applied and the temperature of the extrudate upon exit from the die. It can be seen that even though the alloy is relatively soft and can be easily extruded, the temperature rise during extrusion is quite significant, especially for the low-temperature extrusions where a 35% increase has been recorded. This will definitely affect the mechanical properties of the alloy, because it has been shown (see Section 3.1) that the microstructure is very sensitive to temperature variations. Hence, the alloy should have been extruded at lower strain rates (ram speed 2 to 3 mm sec^{-1}) to allow heat extraction to the surroundings, because the container and the die were maintained at 50° C lower than the desired extrusion temperature.

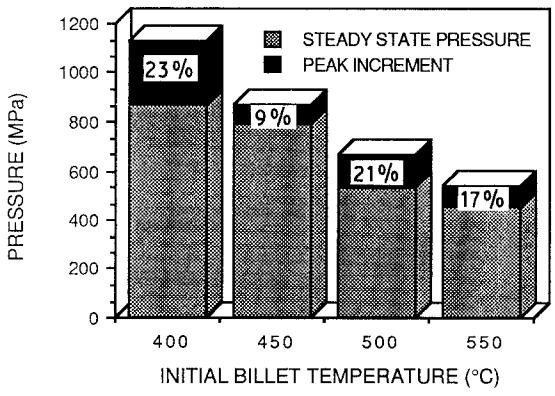

Figure 5 Influence of initial billet temperature on extrusion pressure (steady state pressure and peak increment): extrusion ratio 20 : 1.

3.3. Microstructural characteristics of the as-extruded material

Transmission electron micrographs of the as-extruded materials at 400, 450 and 500° C after quenching are shown in Figs 6a to c, respectively. The following conclusions can be drawn from a closer inspection of the micrographs.

Firstly, the microstructure is fibrous regardless of

TABLE III

	Initial billet temperature (° C)			
	400	450	500	550
Temperature at peak pressure ° C	442	479	520	563
Final extrudate temperature ° C	540	548	561	580

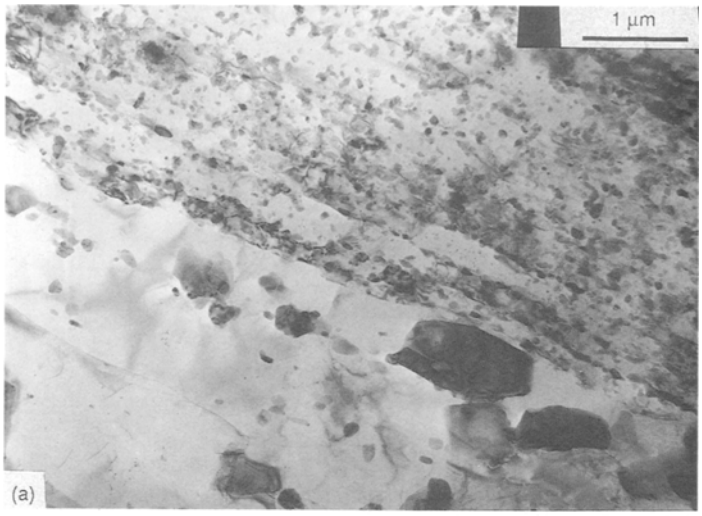

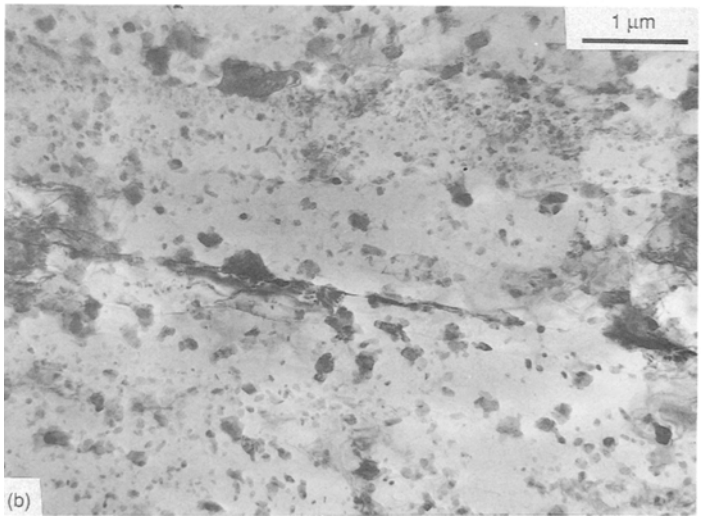

Figure 6 Typical extrudate microstructures (R = 20 : 1): (a) 400° C (TEM); (b) 450° C (TEM); (c) 500° C (TEM); (d) array of second-phase intermetallic particles (TEM).

the processing conditions. This is typical of the as-extruded microstructure because the strains exerted on the powder particles as they pass the intense shear zone during deformation result in bands aligned in the extrusion direction. The microstructure appears to be extremely heterogeneous, composed of coarse and fine zones in intimate contact with each other. The processing parameters, such as extrusion ratio, time and temperature affect the precipitation and coarsening kinetics. Hence, the structure varies according to the control exercised during the thermomechanical extrusion process, and specifically the higher the temperature of deformation and the lower the strain rate the larger will be the grains/subgrains formed. It is thus expected that the microstructure should be uniform and more or less homogeneous. However, due to the short processing times (the whole extrusion process takes less than 10 min) the final developed microstructure depends largely on the as-atomized powder microstructure. Therefore, the heterogeneity of the microstructure can be attributed to the variation in powder particle size, resulting in bands, aligned in the extrusion direction, with different-sized precipitates and subgrains. The size of the bands is restricted by oxide particles formed during atomization and broken up during consolidation. The oxide particles were not visible under all the processing conditions, indicating that the oxide forms small submicrometre particles which are not easily distinguishable from the dispersoids.

The deformation is controlled by dynamic recovery, leading to a substructure of subgrains of low misorientation. The second-phase particles have been very effective as obstacles to dislocation movement, assisting in the formation and stabilization of the substructure, see Fig. 6d. The effect of extrusion temperature on the coarsening of the microstructure is obvious, the structure coarsens progressively as the temperature of the extrusion increases, the precipitates are coarser, situated within the aluminium matrix and on subgrain boundaries. Finally, with increasing extrusion temperature, coarsening of the microstructure creates a profoundly heterogeneous microstructure.

For completeness, X-ray studies were performed and the results of the analysis indicate that, apart from α-Al matrix, the phases detected in the extrudates are the metastable phase(s), and the equilibrium Cr_2Al_{13} phase. The main difference between the X-ray diffraction patterns of the as-atomized powder and the as-extruded material is the intensity of the peaks of the latter compound, which is considerably higher in the as-extruded material than in the as-atomized powder. Hence, it can be concluded that during the thermomechanical process the iron does not form any equilibrium compound and it is almost certain that the

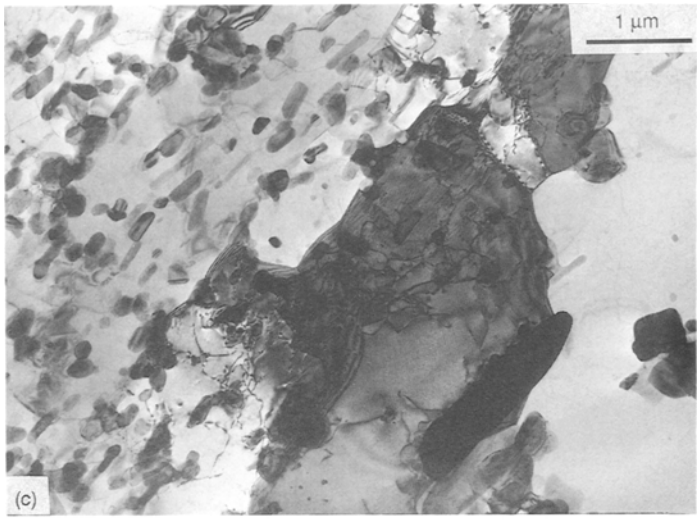

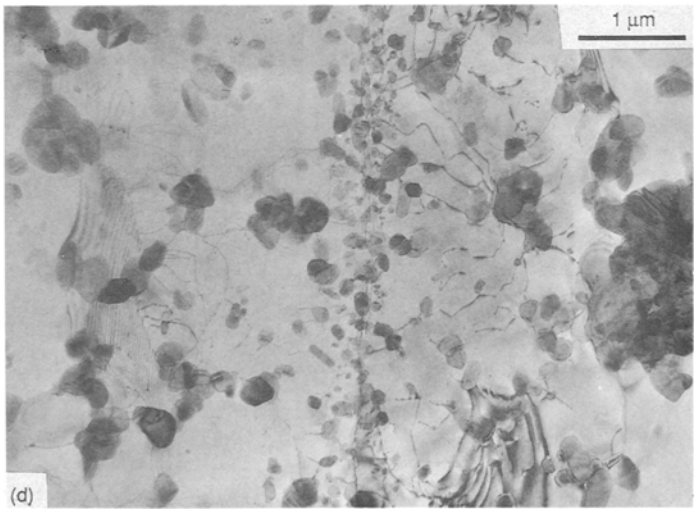

Figure 6 Continued.

unidentified reflections can be assigned to iron-rich phases.

3.4. Mechanical properties of the consolidated product

The mechanical properties of the alloy were evaluated in terms of hardness, 0.2% proof stress, ultimate tensile stress (UTS), elongation to fracture and short-rod fracture toughness. In general, the mechanical properties of an alloy depend on its microstructural features; that is, its subgrain size, grain-boundary morphology and the dispersion of second-phase particles. It is, therefore, obvious that the processing parameters, which affect the microstructure evolved from the thermomechanical extrusion process, will also affect the mechanical properties. The effect the extrusion temperature exerts on the room-temperature mechanical properties is illustrated in Figs. 7a to c. Because the alloy is dispersion hardened, lower consolidation and processing temperatures reduce second-phase particle coarsening, producing higher strengths.

An increase in the extrusion temperature from 400 to 550° C causes a reduction in hardness, 0.2% proof stress and UTS of approximately 12%, 25% and 12% respectively. The decrease in strength is accompanied by an increase in elongation to fracture and fracture toughness of 12% and 14%, respectively. The results reflect the coarsening rate and the potential volume fractions of the respective intermetallic phases. It is well known [14] that the stress required for void initiation is inversely proportional to the particle size. Moreover, it must also be noted that the strength values of this alloy are lower than the target properties of a dispersion strengthened alloy. On the other hand, the elongation to fracture and fracture toughness at high processing temperatures are above the target values. A comparison of the mechanical properties of this alloy and two other dispersion/precipitation strengthened R/S alloys, processed at Imperial College [13] under similar conditions, is presented in Table IV. It can be seen that the Al–5Cr–2Zr exhibits higher strength values, possibly attributable to a dispersion of fine $ZrAl_3$ precipitates, while the cause of the lower fracture toughness may be the higher volume fraction of Cr_2Al_{13}.

The SEM fractographs depict the topography, appearance and specific characteristic features of fracture surfaces. These attributes are manifestations of the various microfracture mechanisms in materials. The fracture surfaces of short-rod fracture specimens tested at ambient temperature of extrudates processed at 400 and 550° C are illustrated in Figs 8 and 9, respectively.

In Fig. 8 it can be seen that the fracture has occurred along fibres corresponding to the original powder particles which are elongated along the

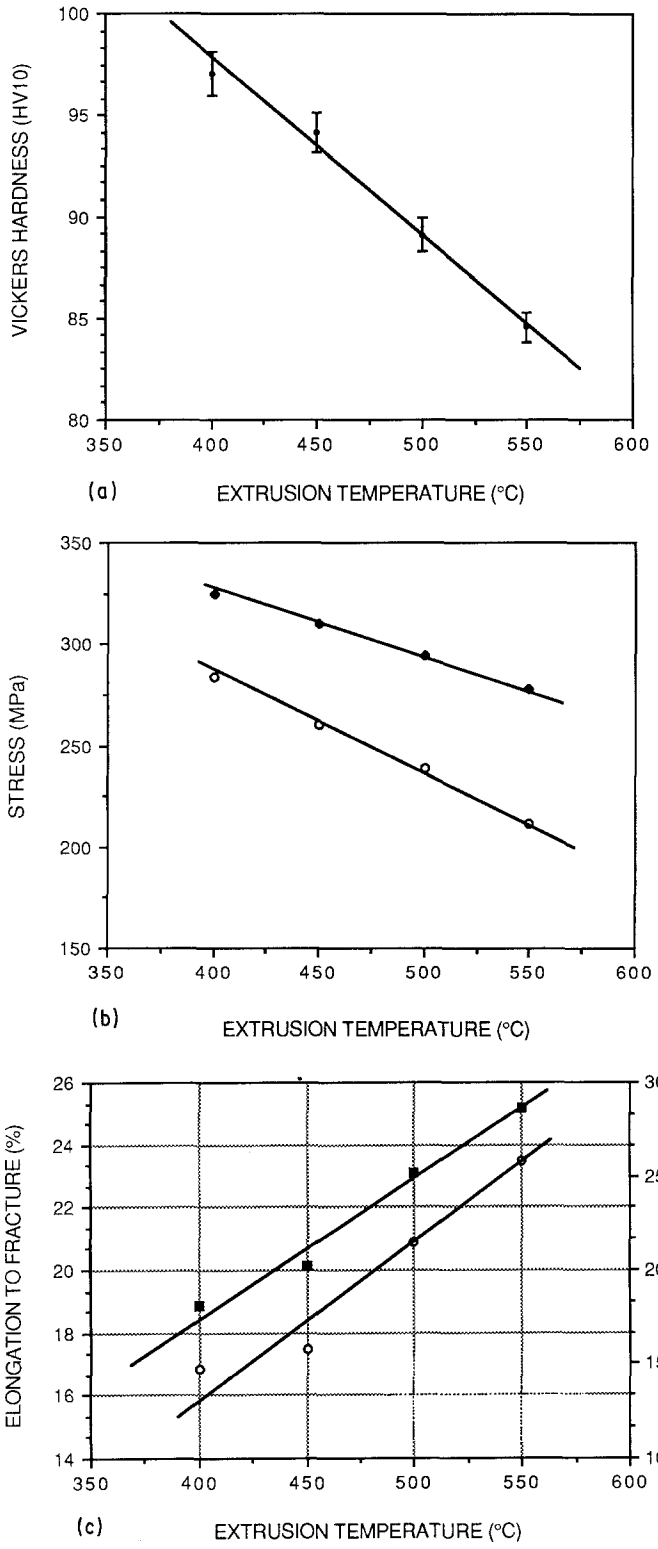

Figure 7 Variation of (a) extrudate hardness, (b) (○) 0.2% proof stress and (◆) UTS, (c) (■) elongation to fracture and (○) short-rod fracture toughness with billet temperature.

extrusion direction, e.g. two spherical powder particles of 20 and 35 μm, extruded at 20:1, would yield fibres of 4.5 and 7.8 μm thickness, and 270 and 472 μm length, respectively. Fig. 10 is a schematic representation of the fracture mechanism of the low-temperature processed extrudate. The features associated with the primary powder particle boundary are the cause of fracture. Obviously oxide particles, forming stringers along primary powder particle boundaries, together with remnants of prior particle boundaries initiate

TABLE IV Tensile properties of extrudates processed at 450° C at 20:1

Alloy	0.2% proof stress (MPa)	UTS (MPa)	Elongation to fracture (%)	Short-rod fracture toughness (MPa $m^{1/2}$)
Al–4Cr–1Fe	260.0 ± 4.7	309.8 ± 0.1	20.1 ± 3.5	15.8 ± 0.6
Al–5Cr–2Zr	396.2 ± 13.3	406.7 ± 6.7	17.9 ± 1.2	11.3 ± 1.2
Al–6.6Cr–1.7Zr	363.0 ± 9.6	369.5 ± 7.8	17.2 ± 1.2	–

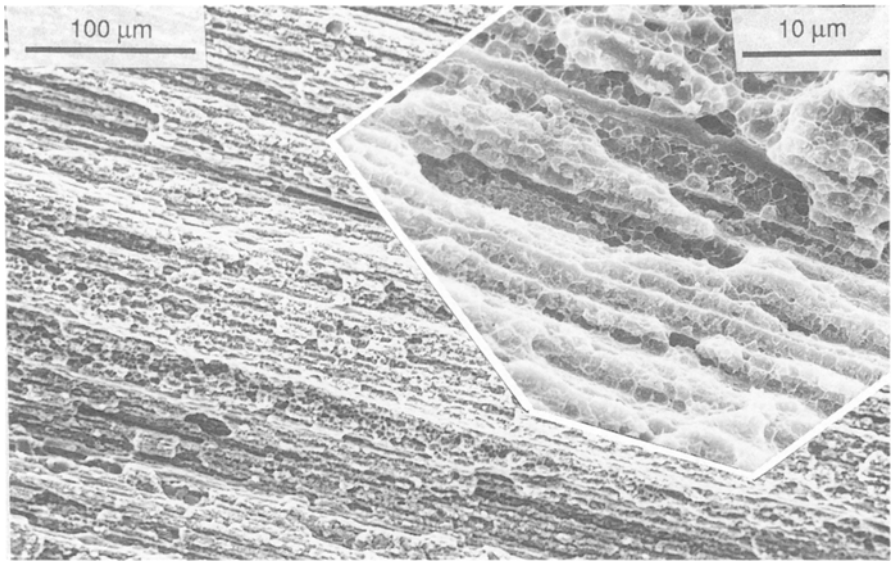

Figure 8 Fracture surface (parallel to extrusion direction) of short-rod fracture toughness specimens of 400° C extrudate (SEM).

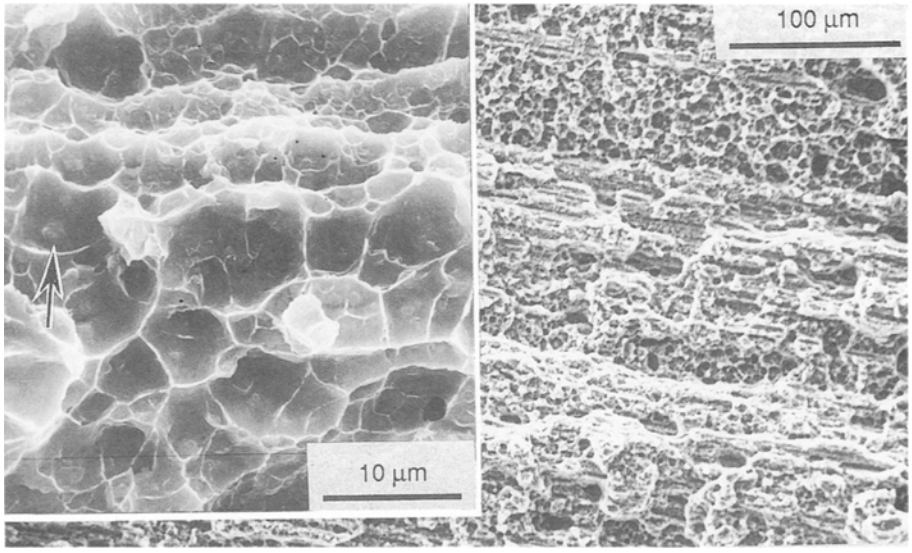

Figure 9 Fracture surface (parallel to extrusion direction) of short-rod fracture toughness specimens of 550° C extrudate (SEM).

void nucleation, thus affecting the fracture behaviour of the consolidated material. Clearly the fracture mode is intergranular along primary powder particles. However, with increasing extrusion temperature this "woody" type of fracture surface disappears; undoubtedly there are signs of secondary failure occurring at primary particle boundaries, but the fracture is mainly transgranular originating at coarse dispersoids, see arrowed example in Fig. 9. A schematic representation of the failure path of the high-temperature processed material (550° C) is given in Fig. 11. Hence the difference in fracture toughness from 14.77 to 25.77 MPa $m^{1/2}$ of extrudates processed at 400 and 550° C, respectively, is attributed to a change in the fracture mode.

Fig. 12 shows the fracture surface of a tensile specimen tested along the longitudinal direction of a 550° C extruded material, whereas Fig. 13 illustrates the fracture mechanism typical of void nucleation at coarse intermetallic particles. The large dimples observed in Fig. 12 (see arrows), could be attributed to some very coarse particles or impurities which were

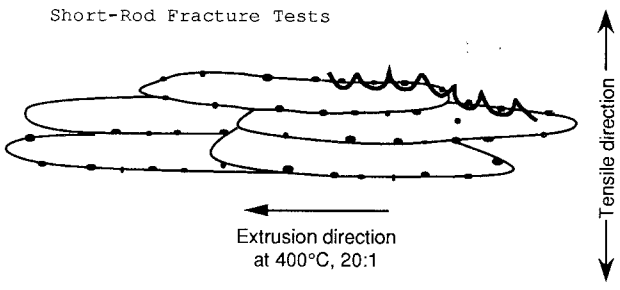

Figure 10 Schematic representation of intergranular failure path (referred to 400° C extrudate).

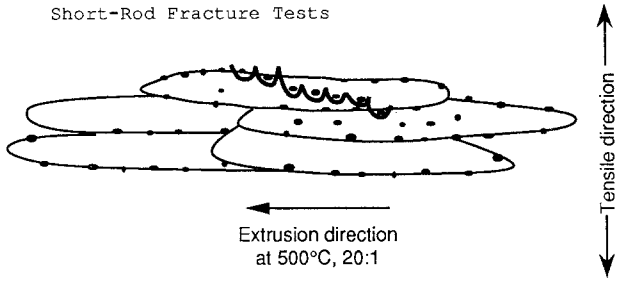

Figure 11 Schematic representation of transgranular failure path (referred to 550° C extudate).

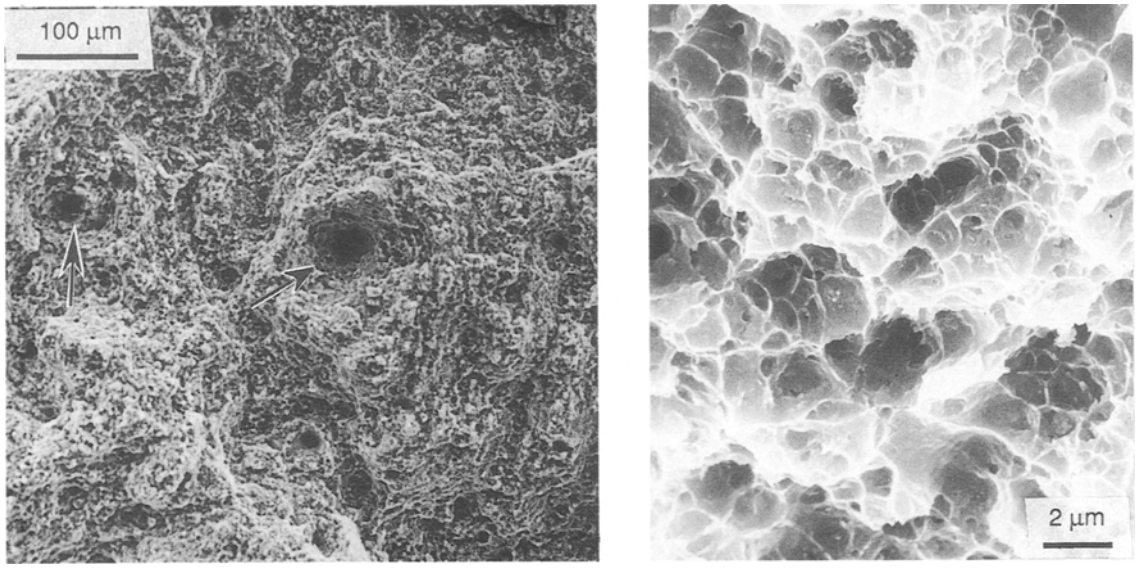

Figure 12 Fracture surface (normal to the extrusion direction) of 550° C extrudate broken in tension (SEM).

preferred nucleants for void formation but they have not affected the fracture mechanism and thus the fracture toughness of the material.

4. Conclusions

The powders exhibited mainly a dual microstructural morphology consisting of a segregation solidification-free rim surrounding the powder particle and cellular morphology with the cells elongated towards the direction of the solidification front.

Decomposition during *in situ* heating of the powder microstructure results in a high volume fraction of mainly globular precipitates. Consolidation takes place during hot extrusion, resulting in a fibrous microstructure composed of bands with different size subgrains originating from different size powder particles. With increasing extrusion temperature the structural inhomogeneity is more profound. The characteristics of the substructure, formed during dynamic recovery, depend on the extrusion temperature, thus affecting the mechanical properties of the as-extruded material. The as-extruded microstructure is similar to the decomposed powder microstructure, where the non-spheroidized plate-like precipitates are aligned in the extrusion direction.

The mechanical properties of this alloy depend upon the processing conditions and mainly upon the extrusion temperature. The values of proof stress and tensile strength are below the target properties of a dispersion-strengthened system. However, due to high values of elongation to fracture and fracture toughness, the alloy used in the present investigation appears to be promising, if it is to be used as, for example, a matrix for a composite material [15]. The fracture surfaces reflect the as-extruded fibrous microstructure, indicating that a lower volume fraction of precipitates with smaller intermetallic particles should give an alloy with improved mechanical properties.

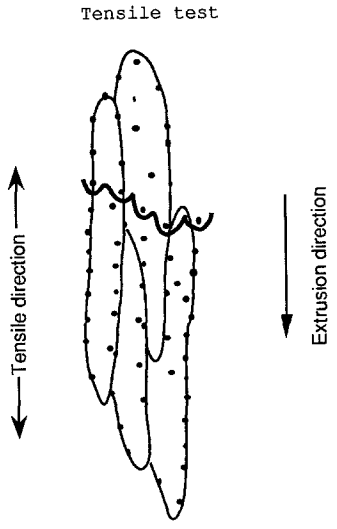

Figure 13 Schematic representation of transgranular failure path (referred to 550° C extrudate broken in tension.

References

1. P. S. GILMAN, *et al.*, presented at the IVth Conference on Rapid Solidification: Processing-principles and Technologies, California, Santa Barbara, 15–18 December 1986.
2. Y-W KIM, in Proceedings of the TMS Symposium "Dispersion Strengthened Aluminium Alloys," edited by Y-W Kim and W. M. Griffith, January 1988, Phoenix, Arizona.
3. C. M. ADAM and R. G. BOURDEAU, in "Proceedings of the 2nd International Conference on Rapid Solidification Processing: Principles and Technologies II," edited by R. Mehrabian, B. Kear and M. Cohen (Claitor's, Baton Rouge, Los Angeles, 1980) pp. 246–59.
4. W. S. MILLER, *et al.*, in "Proceedings of a TMS-AIME Symposium on Aluminium Powder Metallurgy," edited by G. J. Hildeman and M. J. N. Koczak, Fall Meeting, Toronto, Canada, 13 to 17 October 1985, pp. 311–31.
5. G. J. MARSHALL, I. R. HUGHES and W. S. MILLER, *Mater. Sci. Technol.* **2** (1986) 394.
6. E. K. IOANNIDIS, G. J. MARSHALL and T. SHEPPARD, *J. Mat. Sci.* **23** (1988) 1486.
7. M. JACOBS, A. DOGGERT and M. STOWELL, *ibid.* **9** (1974) 1631.
8. W. J. BOETTINGER, L. BENDERSKY and J. G. EARLY, *Met. Trans. A* **17A** (1986) 781.
9. W. S. MILLER and I. G. PALMER, *Metal Powder Rep.* October (1986) 761.
10. E. K. IOANNIDIS, PhD thesis, University of London (1987).

11. L. F. MONDOLFO, *Aluminium Alloys* (Butterworth, London-Boston, 1976).
12. G. J. MARSHALL, E. K. IOANNIDIS and T. SHEPPARD, *Powder Met.* **29** (1986) 57.
13. E. IOANNIDIS and T. SHEPPARD, *Mater. Sci. Tech.* (in press).
14. E. A. STARKE JR, Proceedings of the 6th International Conference on Strength of Metals and Alloys, Melbourne, Australia, August 1982, pp. 1025–44.
15. N. RAGHUNATHAN, E. IOANNIDIS and T. SHEPPARD, *J. Mater. Sci.* (in press).

Received 24 April
and accepted 29 September 1989